Research Article | Vol. 31, No. 12 / 5 Jun 2023 / Optics Express 20256
Optics EXPRESS

# (3+1)D printed adiabatic 1-to-M broadband couplers and fractal splitter networks

ADRIÀ GRABULOSA,[1,*] XAVIER PORTE,[1,2] ERIK JUNG,[1,3] JOHNNY MOUGHAMES,[1] MUAMER KADIC,[1] AND DANIEL BRUNNER[1]

[1] *Institut FEMTO-ST, Université de Franche-Comté - CNRS (UMR 6174), 25030 Besançon, France*
[2] *Currently with Institute of Photonics, Department of Physics, University of Strathclyde, Glasgow G1 1RD, UK*
[3] *Currently with Department of Physics, Heidelberg University, Kirchhoff-Institute for Physics, Im Neuenheimer Feld 227, 69120 Heidelberg, Germany*
[*] *adria.grabulosa@femto-st.fr*

**Abstract:** We experimentally demonstrate, based on a generic concept for creating 1-to-M couplers, single-mode 3D optical splitters leveraging adiabatic power transfer towards up to 4 output ports. We use the CMOS compatible additive (3+1)D *flash*-two-photon polymerization (TPP) printing for fast and scalable fabrication. Optical coupling losses of our splitters are reduced below our measurement sensitivity of 0.06 dB by tailoring the coupling and waveguides geometry, and we demonstrate almost octave-spanning broadband functionality from 520 nm to 980 nm during which losses remain below 2 dB. Finally, based on a fractal, hence self-similar topology of cascaded splitters, we show the efficient scalability of optical interconnects up to 16 single-mode outputs with optical coupling losses of only 1 dB.



## 1. Introduction

Low-loss single-mode optical coupling is a fundamental photonic tool, in both, classical and quantum settings. Several methods have been utilized to address this subject [1], and the most common and well-established techniques include diffraction grating-based optical coupling [2–4], end-fire coupling [5–7] and adiabatic coupling [8,9]. Compared to others, adiabatic coupling can achieve highly efficient and broadband single-mode field-transfer from 1-to-M waveguides using a tapered/inversely-tapered waveguide sequence [10], and it is a widespread technique in current 2D photonic integrated circuits technology [11,12]. Optical transfer between the in- and output waveguides is achieved through evanescent coupling, where the optical mode adiabatically leaks from the core of the tapering input waveguides through the cladding into the inversely-tapering output waveguides [13].

Adiabatically coupled waveguides can be applied for sensing and characterization of on-chip wafer-scale microphotonic components such as microdisk arrays, planar microrings and photonic crystal waveguides [14,15]. Furthermore, this principle has been proposed as an efficient-to-integrate scheme for mode-selective coupling [16,17] in multi-spatial mode optical communications. Generally speaking, it is the back-bone of so-called photonic lanterns [18] with their many applications. The majority of previous studies consider adiabatic coupling between tapered optical fibers and different nanophotonic devices. Single-mode coupling of guided light from a tapered fiber to a photonic waveguide has been achieved with efficiencies up to 97 % [19], representing a promising avenue for integrated photonic circuits [20]. Here, we achieve even lower losses, demonstrating a record transfer efficiency of 98.6 %.

For advantageous scaling of photonic networks, unlocking the third dimension for integration is essential [21]. The reason is that any two-dimensionally integrated photonic circuit that aims at mapping $N$ inputs to $M$ outputs has an area of the order $A \propto N \times M$, i.e. area scales quadratically

#486235 https://doi.org/10.1364/OE.486235
Journal © 2023 Received 26 Jan 2023; revised 31 Mar 2023; accepted 25 Apr 2023; published 1 Jun 2023

Optics EXPRESS

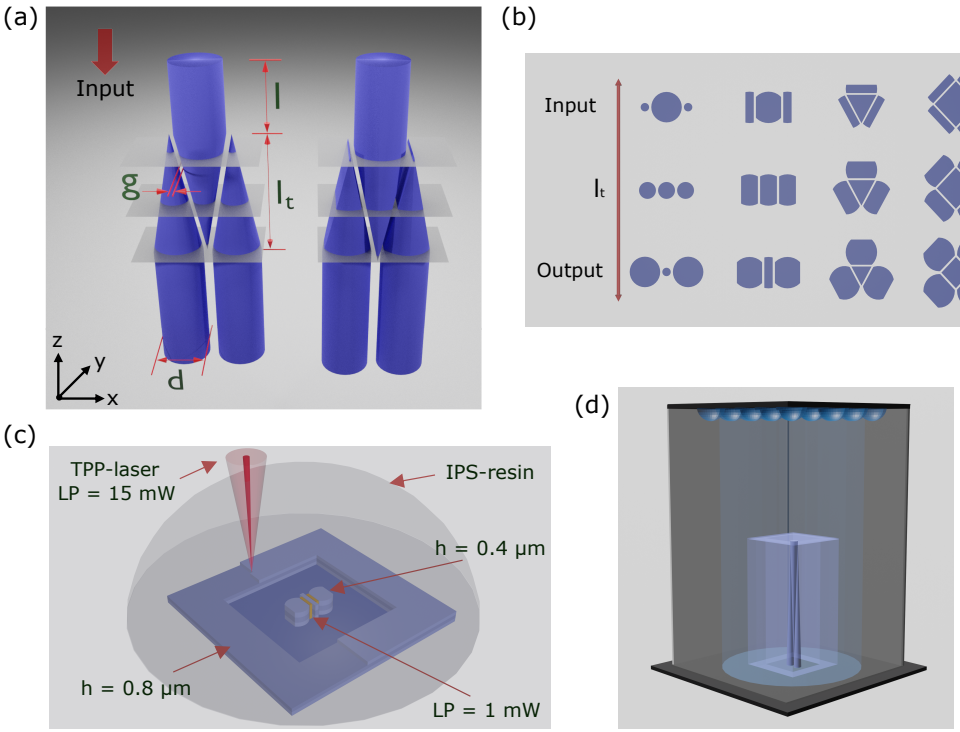


**Fig. 1.** (a) Schematic illustration of conical (left) and truncated rod (right) tapering geometries of 3D-printed optical 1 to 2 splitters. (b) Waveguides' cross-sections along taper-length $l_t$ for adiabatic splitters showing 1 to 2 couplers with conical (left) and truncated rod (right) geometry, followed by 1 to 3 and 1 to 4 truncated rod splitters. (c) Schematic illustration of the (3+1)D *flash*-TPP fabrication. The IP-S photoresist is polymerized via TPP, where the waveguide cores (mechanical supports, e.g. side walls) are printed with hatching distances of $h$ = 0.4 µm ($h$ = 0.8 µm) using a laser power LP = 15 mW. Section in-between waveguides are printed with a lower (LP = 1 mW) TPP power. (d) Once the TPP part of the process is completed and the regions outside the cuboid developed, the structure is introduced in a UV chamber where the unexposed cuboid's inner regions are polymerized via OPP.

with in- and output dimensionality in the typically encountered situation of $N \propto M$ . Using truly 3D integration [22] fundamentally changes the scaling laws, as area and height both scale linearly, which potentially has far-reaching implications for integrating photonic neural networks, Ising machines and other concepts aiming at leveraging the high-dimensionality of photonics [23,24].

Generally, throughput efficiency drops exponentially in a 'deep' circuit that cascades multiple components in series. Parallel and efficient scalability of photonic signals is essential for the future integration of photonic circuits in applications based on large-scale interconnects [20,25]. These require connecting numerous in- and output channels while maintaining parallelism, and fractal topologies for cascading optical splitters have been demonstrated to be a suitable strategy to route optical signals in 3D [26]. Importantly, fractal coupling architectures distribute an input across a number of outputs that exponentially increases with the number of splitters in a signal's pathway, hence losses remain linear relative to the number of output channels. Yet, ultra-low remain of vital importance for scalable large-scale photonic integration of optical quantum networks and repeaters [27,28].

Optics EXPRESS

Here, we experimentally evaluate different tapering strategies in additively (3+1)D-printed [22] single-mode couplers with 1 input and up to 4 outputs. However, the strategy is generally applicable to higher-order splitters. We demonstrate that global losses (injection, coupling and propagation) remain < 2 dB for an exceptionally wide, almost octave-spanning, wavelength range from 520 nm to 980 nm, with only 0.32 dB at optimal conditions. Finally, we show efficient scalability of optical interconnects with fractal topology by cascading individual splitters to exponentially increase the number of optical ports, here connecting 1 input to 16 outputs. Our 3D lithography fabrication technology is additive and CMOS compatible.

## 2. 3D adiabatic 1-to-M couplers design

Using the case of 1 to 2 splitters for illustrating the concept, we tapered waveguide cores according to two different strategies as illustrated in Fig. 1(a), where the left (right) panel shows conical (truncated rod) geometries. In both, the waveguide cross-section continuously changes along the $z$-propagation direction from an input diameter $d$ through a taper-length $l_t$, which is intrinsically linked to the beating length $z_b = \lambda/\Delta n$ [29]. In the conical geometry, the waveguide core shrinks at an equal rate $d/l_t$ along $(x, y)$. In the truncated rod geometry, the core is cut inwards at that rate along $x$, while along $y$ it retains its original shape. Truncated rod tapering restricts coupling to be parallel to the splitting direction, consequently increasing the effective interface-area between the coupled waveguides by purposefully directing the evanescent leakage. Figure 1(b) shows the waveguides' cross-sections along the tapering regions for the different 1-to-M splitters and tapering strategies. To achieve efficient adiabatic overlapping of optical modes, we inversely tapered in- and output waveguides with equal taper-rate and geometric symmetry in order to match the relevant effective modal indices. We separated neighboring waveguides by a gap $g \in \{0.4,\ 0.8,\ 1.2\}$ µm in order to study the evanescence coupling efficiency against the distance between coupled waveguides. Finally, to all output ports we added a straight section with length $l = 30$ µm to minimize cross-talk outside the tapered section. The same tapering strategy was used for fabricating 1 to 3 (1 to 4) splitters, for which triangular (quadrangular) pyramids waveguide cross-sections are required for the truncated rod geometric symmetry for both the 1 to 3 (1 to 4) couplers, see last two illustrations in Fig. 1(b).

## 3. (3+1)D *flash*-TPP fabrication

We leveraged rapid fabrication by combining one- (OPP) and two-photon polymerization (TPP) in the (3+1)D *flash*-TPP lithography concept, schematically illustrated in Fig. 1(c-d), saving up to 90 % of fabrication time [30]. We use the commercial 3D direct-laser writing Nanoscribe GmbH (Photonics Professional GT) system and the liquid negative-tone IP-S photoresist for the fabrication (see Fig. 1(c)). The waveguide cores are printed in a single-step via TPP, with an optimal laser power (LP = 15 mW) and small hatching distance ($h = 0.4$ µm) to ensure smooth surfaces. Furthermore, we polymerized with a low TPP laser power (LP = 1 mW) the volume in-between tapers to ensure a constant gap $g$ throughout that region to establish slight mechanical adhesion between the individual tapers without creating a notable modification of the gap's refractive index. Mechanical supports, i.e. the cuboid's surfaces that define the outer limits of our volumetric circuit, are printed with larger hatching distance ($h = 0.8$ µm). As globally fixed fabrication parameter, the slicing distance is set to $s = 1$ µm since it does not crucially affect optical performance for purely vertical waveguides. After complete-TPP of the IP-S photoresist ($n \approx 1.51$) [31], the unexposed photoresist outside the cuboid is removed following a standard two-step development process. Finally, the entire 3D circuit is UV-blanket exposed, polymerizing the unexposed volume inside the photonic chip via OPP with a UV exposure dose of 3000 mJ/cm$^2$ (see Fig. 1(d)). This provides an auxiliary matrix that improves the stability for complex structures during fabrication without significantly modifying the refractive index contrast ($\Delta n \approx 5 \times 10^{-3}$) [30].

Optics EXPRESS

## 4. Optical performance

We evaluate the performance of the splitters by examining the optical near-field of the output modes as well as the global losses, which include injection, coupling and propagation losses. Figure 2(a) depicts the output intensities of truncated rod optical splitters for 2, 3 and 4 outputs. We generally use $\lambda = 660$ nm for our basic characterization and a core diameter $d = 3.3$ µm that provides high mode confinement within the waveguide core while remaining single-mode [30]. The positioning of the individual intensities matches perfectly with the designed 1-to-M splitters output arrangement (cf. Figure 1(b)), which indicates the high-fidelity of the model and obtained layout. From the output intensity profiles in Fig. 2(b), it is clear that for $l_t = 200$ µm the outputs profiles are not the fundamental $LP_{01}$ mode, and for $g = 1.2$ µm (bottom) individual output modes are not sufficiently decoupled. In contrast, we obtain full splitting of $LP_{01}$ single-modes for $l_t \in \{300,\ 400,\ 500\}$ µm for all $g$. Consequently, the adiabatic criterion of our 1 to 2 splitters is fulfilled for a taper-length $l_t > 200$ µm, which agrees with the theoretical value of $z_b \approx 132$ µm, at injection wavelenght $\lambda = 660$ nm [29].

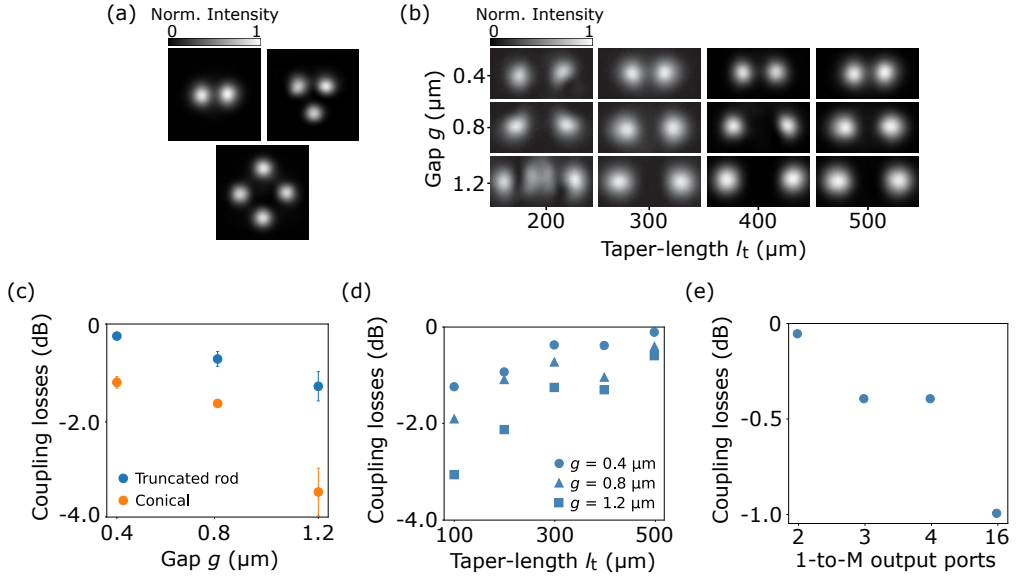


**Fig. 2.** (a) Experimental output intensity profiles of the 1 to 2, 3 and 4 splitters leveraging adiabatic coupling with truncated rod geometry. (b) Output intensity profiles of the 1 to 2 optical splitters for taper-length $l_t \in \{200,\ 300,\ 400,\ 500\}$ µm (left to right) and gap distances $g \in \{0.4,\ 0.8,\ 1.2\}$ µm (top to bottom). (c) Coupling losses versus gaps $g \in \{0.4,\ 0.8,\ 1.2\}$ µm for 1 to 2 splitters with conical (blue) and truncated rod (orange) geometry and taper's length $l_t = 300$ µm. (d) Coupling losses of 1 to 2 splitters with truncated rod geometry for gaps $g$ and taper-lengths $l_t \in \{100 : 100 : 500\}$ µm. (e) Coupling losses versus number of output ports for the different 1-to-M adiabatic splitters with truncated rod geometry, i.e. 1 to 2, 1 to 3, 1 to 4 and cascaded 1 to 16.

The adiabaticity criterion was numerically validated by 2D-simulations via COMSOL Multiphysics. There, the fundamental eigenmode is launched at the waveguide's input facet via *Port* boundary conditions, and then propagated throughout a 2D projection of the splitters from Fig. 1(a) with scattering boundary conditions and $\Delta n \approx 5 \times 10^{-3}$. This further confirms the adiabatic signature of our truncated rod 3D optical splitters.

We characterized the global losses of 1 to 2 splitters with conical and truncated rod geometry for different gaps $g \in \{0.4,\ 0.8,\ 1.2\}$ µm. Previously we determined injection losses of 0.26 dB for

Optics EXPRESS

waveguides with the same characteristics [30], which we use to extract the propagation-coupling losses of our optical splitters. As observed in Fig. 2(c), the truncated rod splitters have lower coupling losses compared to the conical case for all gaps $g \in \{0.4,\ 0.8,\ 1.2\}$ µm. This better performance is presumably due to the extra directionality and increased effective transfer-area and we therefore select the truncated rod geometry for the following investigations. Figure 2(d) shows the coupling losses of the 1 to 2 splitters with truncated rod geometry for different gaps $g \in \{0.4,\ 0.8,\ 1.2\}$ µm, where we scan taper-length $l_t$ from 100 to 500 µm. We find optimal coupling behavior for $l_t = 500$ µm and $g = 0.4$ µm, with global losses of 0.32 dB and correspondingly ultra-low coupling losses of only 0.06 dB. Intensities at the two output ports differ only by ~ 3.4 %. Finally, using optimal $l_t = 500$ µm and $g = 0.4$ µm, we fabricated 1 to 3 and 1 to 4 splitters (cf. Figure 2(a)) with coupling losses of only 0.4 dB and intensity difference between output ports of ~4.6 % (~6.1 %) for 1 to 3 (1 to 4) splitters. Coupling losses for the 1 to 3 and 1 to 4 splitters are hence close to identical. Figure 2(e) depicts the coupling losses versus number of output ports for the different 1-to-M adiabatic splitters.

## 5. Broadband functionality

A major advantage of adiabatic power transfer compared to interference-based directional couplers is a substantially lower wavelength-sensitivity of splitting ratios [32,33]. We test the broadband functionality of our 1 to 2 optical splitters with $l_t = 500$ µm by injecting different wavelengths ranging from $\lambda = 520$ nm to $\lambda = 980$ nm. Crucially, the bulk absorption of the IP-S photoresist does not play a role on our short relevant length $l_t$ across the entire wavelength range investigated here [31]. According to data shown in Fig. 3(a), global losses remain below 2 dB for the 1 to 2 splitters over this range almost spanning an octave. For $\lambda \geq 660$ nm, global losses start to increase due to lower modal confinement for which larger gap $g$ is required for adiabaticity. At $\lambda = 520$ nm, we approach the single-mode cut-off wavelength, which lies at $\sim \lambda = 480$ nm. Higher-order modes begin to be excited for which the evanescent coupling decreases due to reduced modal overlap. Finally, Fig. 3(b) depicts the output intensity profiles of the splitters across this entire range of wavelengths, which clearly show the discussed effects appearing higher-order modes as well as non-separated single-modes. We attribute this to the dispersion relation of the IP-S photoresist [31], which makes optical confinement to the waveguide's core wavelength dependent. This, in turn modifies the optimal coupling distance for adiabaticity.

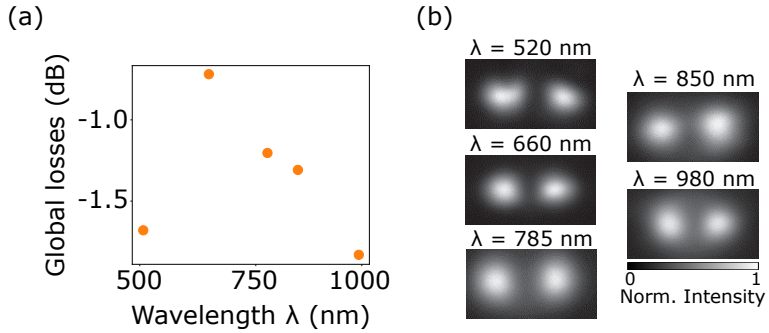


**Fig. 3.** (a) Global losses versus injection light wavelength $\lambda$ of the 1 to 2 splitters with $l_t = 500$ µm and $g = 0.8$ µm. (b) Output intensity profiles from (a) over $\Delta\lambda \sim 500$ nm.

## 6. Fractal networks of 3D splitters

An efficient way of distributing information across many channels is leveraging fractal, i.e. self-similar branching topologies [26]. In such fractal architectures, sequential layers follow

Optics EXPRESS

similar patterns at various scales and successive magnifications. This means that the tree's architecture is defined according to the spacing between the output waveguides $D_L$ and height $H_L$, where $L$ is the number of the particular bifurcation layers. To this aim, the dimensions throughout the bifurcation layers 'scale' as $D_l = \sqrt{b}\, D_{(l+1)}$ and $H_l = \sqrt{b}\, H_{(l+1)}$, where $b$ represents the number of splitting branches. For the case of our 1 to 16 splitters, i.e. cascading 1 to 4 splitters ($l_t$ = 500 μm, $g$ = 0.4 μm) in a double-layer, results in $b$ = 4 splitting branches, and $D_L$ and $H_L$ double each consecutive layer. There, the outputs of a 1-to-M splitter act as the inputs to another splitter with the same splitting ratio. In such geometries, the number of output channels scales exponentially with the number of splitters cascaded in a sequence. Here, we cascaded 1 to 4 splitters in two layers, where there are (is) one (four) couplers(s) in the first (second) layer. This realizes 16 output ports, and Fig. 4(a) schematically illustrates the design. Ports between the two layers are linked via bent waveguides following a cosine-like shape with $D_1$ = 10 μm, $H_1$ = 200 μm, $D_2$ = 20 μm and $H_2$ = 400 μm as labeled in Fig. 4(a).

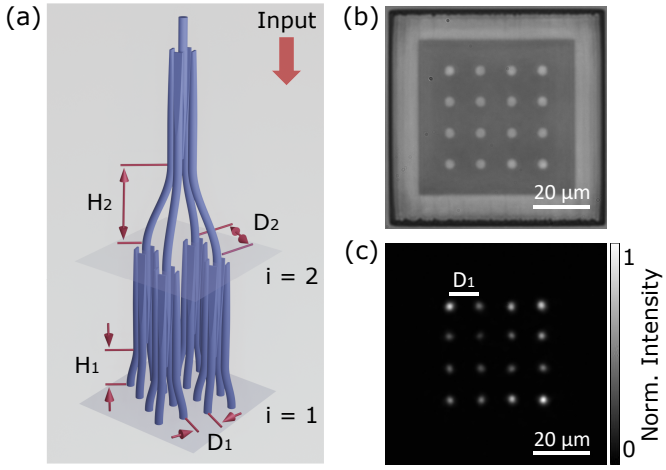


**Fig. 4.** (a) Design of the cascaded 1 to 16 optical splitters with truncated rod geometry. (b) Optical microscope image showing the output (bottom surface) of the structure integrating the cascade 1 to 16 splitters. (c) Output intensity profiles from (a-b).

Figure 4(b) and (c) show an optical microscope image of the output facet under incoherent illumination and the optical output of the 1 to 16 coupler, respectively. Coupling losses are only 1 dB (see Fig. 2(e)), and each individual output is single-mode. The cascaded 1 to 16 coupler therefore performs slightly better than the individual splitters, considering the propagation losses of the bent waveguides in the output ports [30,34]. Currently we attribute this to slight variations in the fabrication process and it is a matter of ongoing investigation.

We find the uniformity of splitting ratios reduced compared to the individual splitters. On average, each output contains (5.81 ± 2.31) % of the injected intensity, which very close to the ideal 6.25 %. Yet, the individual coupling ratios to the 16 output waveguides do deviate from this average value considerably.

## 7. Conclusion and outlook

In summary, we have shown (3+1)D *flash*-TPP fabrication of single-mode 3D optical splitters leveraging adiabatic power transfer between one input and up to 4 output ports. After optimization of the device geometry, comparing conical and truncated rod tapering geometries, we obtain record 0.32 dB (0.06 dB) global (coupling) losses for the truncated geometry of 1 to 2 splitters with only ~ 3.4 % difference between two output port intensities. We evaluated their wavelength

Optics EXPRESS

dependency, and found them to be very broadband, with global losses remaining below < 2 dB over almost an octave-spanning range from 520 nm ≤ $\lambda$ ≤ 980 nm.

We continued to demonstrate efficient scalability of optical interconnects by cascading 1 to 4 optical splitters in a fractal topology, creating 16 output ports with low optical coupling losses of 1 dB (see Fig. 2(e)). Currently, the splitting ratio of the cascade couplers does still exhibit notable variations, and further efforts to improve the splitting homogeneity should investigate potential refractive index or thickness variations of the gap separating the tapers and inverse tapers. Other concepts, such as multi-mode interferometer-based coupling structures [35,36] result in complex designs based on intensive numerical calculations during performance optimization. Furthermore, just like directional couplers, their ratios strongly vary with the input wavelength. As such, the adiabatic power transfer concept features some highly interesting properties.

Additionally, the possibility of separating output ports via bent waveguides opens new avenues to create integrated hybrid systems by combining our polymer-based single-mode splitters with semiconductor lasers, such as quantum dot micropillars arrays [37,38].

Photonic circuits hold a big promise for future parallel and scalable optical interconnects [26], particularly considering the size of modern neural network concepts. As here demonstrated, further reducing the gap between in- and output waveguides could be beneficial in terms of coupling losses (cf. Figure 2(d)) as well as integration compactness. However, the minimal lateral distance for resolvable modification of neighboring voxels, given by the generalized two-photon Sparrow criterion [39], sets a fundamental limitation. For a fs-laser operating at $\lambda$ = 780 nm and a microscope objective with NA = 0.8, the minimum lateral separation is 0.344 μm, which agree well with the $g$ = 0.4 μm used in our investigations.

An interesting approach to reduce the taper-length $l_t$, while maintaining a constant gap, leverages short-cuts for adiabaticity [40]. This strategy relies on adapting concepts of quantum control theory for light manipulation in optical devices and waveguide optics [41–43]

Photonic integration is a promising approach to reduce the power consumption of neural network computing hardware, yet scalability of integration concepts is essential [44] and simultaneously hard to achieve. Such scalability is not achievable in 2D circuits [44], and 3D photonic integration might proof essential. Importantly, all used resins and processes are CMOS compatible, full-filling an important prerequisite for synergistic combinations of electronic and photonic circuits.

**Funding.** Horizon 2020 Framework Programme (713694); Volkswagen Foundation (NeuroQNet II);Agence Nationale de la Recherche (ANR-17-EURE-0002, ANR-15-IDEX-0003); Conseil régional de Bourgogne-Franche-Comté; French Investissements d'Avenir.

**Acknowledgments.** This word was partially supported by the French RENATECH network and its FEMTO-ST technological facility.

**Disclosures.** The authors declare no conflicts of interest.

**Data availability.** Data underlying the results presented in this paper are not publicly available at this time but may be obtained from the authors upon reasonable request.

## References

1. G. Son, S. Han, J. Park, K. Kwon, and K. Yu, "High-efficiency broadband light coupling between optical fibers and photonic integrated circuits," Nanophotonics **7**(12), 1845–1864 (2018).
2. A. Bozzola, L. Carroll, D. Gerace, I. Cristiani, and L. C. Andreani, "Optimising apodized grating couplers in a pure soi platform to −0.5 db coupling efficiency," Opt. Express **23**(12), 16289–16304 (2015).
3. M. L. Dakss, L. Kuhn, P. F. Heidrich, and B. A. Scott, "Grating coupler for efficient excitation of optical guided waves in thin films," Appl. Phys. Lett. **16**(12), 523–525 (1970).
4. S. Peng and T. Tamir, "Directional blazing of waves guided by asymmetrical dielectric gratings," Opt. Commun. **11**(4), 405–409 (1974).
5. C. H. Bulmer, S. K. Sheem, R. P. Moeller, and W. K. Burns, "High-efficiency flip-chip coupling between single-mode fibers and linbo3 channel waveguides," Appl. Phys. Lett. **37**(4), 351–353 (1980).
6. W. K. Burns and G. B. Hocker, "End fire coupling between optical fibers and diffused channel waveguides," Appl. Opt. **16**(8), 2048–2050 (1977).

Optics EXPRESS


7. J. Noda, O. Mikami, M. Minakata, and M. Fukuma, "Single-mode optical-waveguide fiber coupler," Appl. Opt. **17**(13), 2092–2096 (1978).
8. S. M. Spillane, T. J. Kippenberg, and K. J. Vahala, "Ultralow-threshold raman laser using a spherical dielectric microcavity," Nature **415**(6872), 621–623 (2002).
9. L. Collot, V. Lefèvre-Seguin, M. Brune, J. M. Raimond, and S. Haroche, "Very high-q whispering-gallery mode resonances observed on fused silica microspheres," Europhys. Lett. **23**(5), 327–334 (1993).
10. A. Dewanjee, J. N. Caspers, J. S. Aitchison, and M. Mojahedi, "Demonstration of a compact bilayer inverse taper coupler for si-photonics with enhanced polarization insensitivity," Opt. Express **24**(25), 28194–28203 (2016).
11. R. Marchetti, C. Lacava, L. Carroll, K. Gradkowski, and P. Minzioni, "Coupling strategies for silicon photonics integrated chips," Photonics Res. **7**(2), 201–239 (2019).
12. T. Tsuchizawa, K. Yamada, H. Fukuda, T. Watanabe, J. ichi Takahashi, M. Takahashi, T. Shoji, E. Tamechika, S. Itabashi, and H. Morita, "Microphotonics devices based on silicon microfabrication technology," IEEE J. Sel. Top. Quantum Electron. **11**(1), 232–240 (2005).
13. A. Snyder, "Coupling of modes on a tapered dielectric cylinder," IEEE Trans. Microwave Theory Tech. **18**(7), 383–392 (1970).
14. P. E. Barclay, K. Srinivasan, M. Borselli, and O. Painter, "Efficient input and output fiber coupling to a photonic crystal waveguide," Opt. Lett. **29**(7), 697–699 (2004).
15. C. P. Michael, M. Borselli, T. J. Johnson, C. Chrystal, and O. Painter, "An optical fiber-taper probe for wafer-scale microphotonic device characterization," Opt. Express **15**(8), 4745–4752 (2007).
16. N. Riesen and J. D. Love, "Tapered Velocity Mode-Selective Couplers," J. Lightwave Technol. **31**(13), 2163–2169 (2013).
17. N. Riesen and J. D. Love, "Ultra-Broadband Tapered Mode-Selective Couplers for Few-Mode Optical Fiber Networks," IEEE Photonics Technol. Lett. **25**(24), 2501–2504 (2013).
18. T. A. Birks, I. Gris-Sánchez, S. Yerolatsitis, S. G. Leon-Saval, and R. R. Thomson, "The photonic lantern," Adv. Opt. Photonics **7**(2), 107–167 (2015).
19. T. G. Tiecke, K. P. Nayak, J. D. Thompson, T. Peyronel, N. P. de Leon, V. Vuletić, and M. D. Lukin, "Efficient fiber-optical interface for nanophotonic devices," Optica **2**(2), 70–75 (2015).
20. N. Lindenmann, G. Balthasar, D. Hillerkuss, R. Schmogrow, M. Jordan, J. Leuthold, W. Freude, and C. Koos, "Photonic wire bonding: a novel concept for chip-scale interconnects," Opt. Express **20**(16), 17667–17677 (2012).
21. J. Moughames, X. Porte, L. Larger, M. Jacquot, M. Kadic, and D. Brunner, "3d printed multimode-splitters for photonic interconnects," Opt. Mater. Express **10**(11), 2952–2961 (2020).
22. X. Porte, N. U. Dinc, J. Moughames, G. Panusa, C. Juliano, M. Kadic, C. Moser, D. Brunner, and D. Psaltis, "Direct (3+1)D laser writing of graded-index optical elements," Optica **8**(10), 1281 (2021).
23. Y. Shen, N. Harris, and S. Skirlo, "Deep learning with coherent nanophotonic circuits," Nat. Photonics **11**(7), 441–446 (2017).
24. J. Felfmann, M. Youngblood, and M. Karpov, "Parallel convolutional processing using an integrated photonic tensor core," Nature **589**(7840), 52–58 (2021).
25. P. Lalanne and P. Chavel, *Perspectives for Parallel Optical Interconnects* (Springer Science and Business Media, 1993).
26. J. Moughames, X. Porte, M. Thiel, G. Ulliac, L. Larger, M. Jacquot, M. Kadic, and D. Brunner, "Three-dimensional waveguide interconnects for scalable integration of photonic neural networks," Optica **7**(6), 640 (2020).
27. R. Van Meter, T. D. Ladd, A. G. Fowler, and Y. Yamamoto, "Distributed quantum computation architecture using semiconductor nanophotonics," Int. J. Quantum Inf. **08**(01n02), 295–323 (2010).
28. H. J. Kimble, "The quantum internet," Nature **453**(7198), 1023–1030 (2008).
29. A. W. Snyder and J. D. Dove, *Optical Waveguide Theory* (Chapman and Hall, 1983).
30. A. Grabulosa, J. Moughames, X. Porte, and D. Brunner, "Combining one and two photon polymerization for accelerated high performance (3 + 1)d photonic integration," Nanophotonics **11**(8), 1591–1601 (2022).
31. M. Schmid, D. Ludescher, and H. Giessen, "Optical properties of photoresists for femtosecond 3d printing: refractive index, extinction, luminescence-dose dependence, aging, heat treatment and comparison between 1-photon and 2-photon exposure," Opt. Mater. Express **9**(12), 4564 (2019).
32. Y. Luo, Y. Yu, and M. Ye, "Integrated dual-mode 3db power coupler based on tapered directional coupler," Sci. Rep. **6**(1), 23516 (2016).
33. G. F. R. Chen, J. R. Ong, and T. Y. L. Ang, "Broadband silicon-on-insulator directional couplers using a combination of straight and curved waveguide sections," Sci. Rep. **7**(1), 7246 (2017).
34. A. Grabulosa, X. Porte, J. Moughames, and D. Brunner, "(3+1)D-printed adiabatic 1-to-N couplers," in *Emerging Topics in Artificial Intelligence (ETAI) 2022*, vol. 12204 G. Volpe, J. B. Pereira, D. Brunner, and A. Ozcan, eds., International Society for Optics and Photonics (SPIE, 2022), p. 1220404.
35. J. Kim, J.-Y. Kim, J. Yoon, H. Yoon, H.-H. Park, and H. Kurt, "Experimental demonstration of inverse-designed silicon integrated photonic power splitters," Nanophotonics **11**(20), 4581–4590 (2022).
36. R. Bruck, K. Vynck, P. Lalanne, B. Mills, D. J. Thomson, G. Z. Mashanovich, G. T. Reed, and O. L. Muskens, "All-optical spatial light modulator for reconfigurable silicon photonic circuits," Optica **3**(4), 396–402 (2016).
37. T. Heuser, J. Große, A. Kaganskiy, D. Brunner, and S. Reitzenstein, "Fabrication of dense diameter-tuned quantum dot micropillar arrays for applications in photonic information processing," APL Photonics **3**(11), 116103 (2018).

Optics EXPRESS

38. A. Grabulosa, J. Moughames, X. Porte, M. Kadic, and D. Brunner, "Additive 3d photonic integration that is cmos compatible," Nanotechnology (2023).
39. J. Fischer and M. Wegener, "Three-dimensional optical laser lithography beyond the diffraction limit," Laser Photonics Rev. **7**(1), 22–44 (2013).
40. D. Guéry-Odelin, A. Ruschhaupt, A. Kiely, E. Torrontegui, S. Martínez-Garaot, and J. G. Muga, "Shortcuts to adiabaticity: Concepts, methods, and applications," Rev. Mod. Phys. **91**(4), 045001 (2019).
41. V. Evangelakos, E. Paspalakis, and D. Stefanatos, "Efficient light transfer in coupled nonlinear triple waveguides using shortcuts to adiabaticity," Sci. Rep. **13**(1), 1368 (2023).
42. S.-Y. Tseng, R.-D. Wen, Y.-F. Chiu, and X. Chen, "Short and robust directional couplers designed by shortcuts to adiabaticity," Opt. Express **22**(16), 18849–18859 (2014).
43. H.-C. Chung, S. Martínez-Garaot, X. Chen, J. G. Muga, and S.-Y. Tseng, "Shortcuts to adiabaticity in optical waveguides," Europhys. Lett. **127**(3), 34001 (2019).
44. K. Boahen, "Dendrocentric learning for synthetic intelligence," Nature **612**(7938), 43–50 (2022).